Carbohydrate Polymer Technologies and Applications 7 (2024) 100450

Contents lists available at ScienceDirect

Carbohydrate Polymer Technologies and Applications

journal homepage: www.sciencedirect.com/journal/carbohydrate-polymer-technologies-and-applications

# Graphene quantum dots/cellulose nanocrystal inclusion complex for enhancing the physical and thermal properties of HDPE polymer matrix

Dilpreet S. Bajwa [a,*], Saptaparni Chanda [a], Cecily Ryan [a], Sreekala G. Bajwa [a], Nicole Stark [b], Kirsten Matteson [a]

[a] Montana State University, Bozeman, MT, USA
[b] USDA Forest Products Laboratory, Madison, WI, USA

ARTICLE INFO

*Keywords:*
Cellulose nanocrystal
High-density poly(ethylene)
Graphene quantum dots
Inclusion complex
Bio-based nanofillers

ABSTRACT

Cellulose nanocrystals (CNC) are desirable material due to universal accessibility, and superior mechanical properties. A major challenge is non-uniform dispersion of CNC in the hydrophobic matrices due to their tendency to agglomerate. A novel technique was evaluated to prepare a hybrid system of cellulose nanocrystal (CNC)/graphene quantum dots (GQD). Hybrid system of CNC/GQD was added to high density poly (ethylene) (HDPE) to manufacture composites. The CNC/GQD inclusion complex properties were evaluated using Zeta potential measurement, Raman spectroscopy, X-ray photoelectron spectroscopy (XPS) and X-ray diffraction (XRD) analysis. The composite properties were analysed using scanning electron microscopy (SEM), thermogravimetric analysis (TGA), differential scanning calorimetry (DSC), dynamic mechanical analysis (DMA), and tensile testing and analysis of electrical impedance spectra. Raman spectroscopy, XPS and XRD confirmed the interaction of CNC and GQD. The SEM micrographs of the cross-sections of GQD induced composites showed a uniform honeycomb like morphology and no sign of agglomeration. GQD incorporated composites exhibited better thermal stability and higher elastic modulus than neat HDPE. The composites showed a purely capacitive response for an AC electrical system measured over 4 Hz to 1 MHz. The results indicate significantly improved dispersion of CNC in the polymer matrix, compared to unmodified CNCs.

## 1. Introduction

Over the past few years, both scientific and industrial communities have given their special attention to the sector of biodegradable and renewable materials, because of their potential to mitigate the impending danger of global warming and pollution. One of the most abundant bio-based polymers is cellulose and it has been used for years in different industries as a potential biodegradable and renewable material. Nanostructured cellulose materials have become a new field of interest in the past few decades, due to their excellent physical and chemical properties., CNCs have garnered special attention amongst the nanocellulose materials because of their superior properties such as: light weight, transparency, high crystallinity (54-88%), excellent mechanical properties- (tensile strength ~ 7 GPa, elastic moduli ~150 GPa), tunable surface properties and of relatively low cost (Angles & Dufresne, 2001; Eichhorn & Davies, 2006; Habibi, 2014; Habibi et al., 2010; Iwamoto et al., 2007; Kargarzadeh et al., 2017; Moon et al., 2011).

The transfer of the exceptional mechanical properties of CNCs from nanoscale level to the macroscale of bulk composites is the most difficult challenge faced during composite processing. Improved dispersion of CNCs and optimized filler-matrix interaction are the only ways to achieve superior mechanical properties (Oksman et al., 2016; Shojaeiarani et al., 2021), and the surface modification processes help to accomplish that. Several chemical non-covalent surface modifications have been achieved using adsorption of surfactants, or oppositely charged moieties. CNC treatment like sulfonation, TEMPO-mediated oxidation, esterification, etherification, silyation, urethanizaiton, amidation, polymer grafting has been evaluated (Habibi, 2014; Kargarzadeh et al., 2017). So far, these chemical modifications have achieved limited success, their full potential has not been achieved in practical applications.

Graphene quantum dot (GQD) is a new class of carbon-based materials. A single layer of $sp^2$-hybridised carbon atoms which are arranged in a honeycomb lattice is called graphene (Sun et al., 2013). Chopped fragments of a few graphene sheets of <10 nm lateral dimension and

* Corresponding author.
*E-mail address:* Dilpreet.bajwa@montana.edu (D.S. Bajwa).

https://doi.org/10.1016/j.carpta.2024.100450

Available online 7 February 2024

<10 graphene layers form GQD particles (Lv et al., 2018). High photostability, thermal and chemical stability, low cytotoxicity, strong photoluminescence, excellent dispersion in water and biocompatibility, fluorescence, and dimensional and morphological tunability are the main reasons to use GQDs for various applications (Kumar et al., 2017; Liu et al., 2021). Due to these excellent properties, GQDs are conventionally used in biomedicine, energy, and photo sensing electronics (Gobi et al., 2017; Guo et al., 2017; Xiong et al., 2019). Nevertheless, their role as dispersing agent for polymer composites is yet to be explored.

In the past few years, GQD/nanocellulose complex has been used in the production of functional hydrogels (Song et al., 2015), thin films (Rosddi et al., 2020) or composites (Ikram et al., 2022) for different applications. The reaction mechanism between CNC and GQD is very complex in nature. GQDs have different chemical groups on the edges. Their lateral dimensions are larger than their heights and are anisotropic in nature (Junka et al., 2014). The basal planes of GQDs are hydrophobic and the edges are hydrophilic because of the presence of carboxylic acid groups (Sekiya et al., 2014). The surface hydroxyl groups of CNC and carboxylic acid groups of GQDs can form hydrogen bonds among themselves exhibiting hydrophobic interactions. Moreover, there is a negative charge on the surface of CNCs due to the hydroxyl groups (Khabibullin et al., 2017; Rodell et al., 2015). The working hypothesis is that the mutual electrostatic repulsion between GQDs and CNCs can improve the dispersion and reduce the agglomeration of CNCs in a polymer matrix.

Inspired by these findings, the objective of this work is to develop an eco-friendly and a sustainable technology for CNC functionalization using GQD to improve the dispersion of CNCs in high-density polyethylene (HDPE) matrix and enhance the overall physical and mechanical properties of the composites. The presence of oxygen containing functional groups on the surface of CNC and GQD facilitates the formation of the CNC/GQD inclusion complex which can be used as reinforcement for HDPE based composites.

## 2. Experimental section

### 2.1. Materials

High-density poly (ethylene) (HDPE) in the powder form with a melt flow index of 3.5 g/10 min, and a melting temperature of 126 °C, was purchased from Nova Chemicals (Calgary, AB, Canada). USDA Forest Products Laboratory (Madison, WI, USA) provided the CNCs. The length of the CNC is within a range of 80-100 nm, width of 10-15 nm, and the aspect ratios of 5-10. The CNCs were extracted from softwood pulp using the sulfuric acid hydrolysis process. Hydrothermal treatment was used to disulfate the CNCs. The aqueous graphene quantum dot (GQD) of blue luminescent was purchased from Sigma Aldrich (St. Louis, MO, USA). The concentration of the aqueous dispersion of GQD was 1 mg/mL, the full-width half maximum (FWHM) of GQD was 60-80 nm, topographic height was 1-2.0 nm, diameter was <10 nm, and functional groups present in the GQD structure were -COOH, -OH, -$NH_2$. Deionized (DI) water was used as a solvent and purchased from Millipore (St. Louis, MO, USA).

### 2.2. Synthesis of CNC/GQD inclusion complex

The reaction between CNC and GQD for the formation of inclusion complex was done as reported in literature (Xiong et al., 2019). Four beakers were taken for preparing four different formulations and 100 mL of DI water was poured in each beaker. One gram of dry mass of CNC was dissolved separately in four beakers. This is the first step, and it was done at room temperature (25°C). In the second step, GQD sol was added in different concentrations in each beaker except one. The concentrations of GQD were 0.01 g, 0.015 g and 0.02 g, respectively. In other words, the volumes of aqueous dispersions of GQD added to the beakers are 10 mL, 20 mL, and 30 mL, respectively. In the fourth beaker, no GQD was added. To do comparative studies of the effect of quantum dot treatment on the dispersion behavior of CNC and the mechanical properties of the resultant composites, the last formulation was used. The GQD containing solutions were stirred for 30 min. In the third step, all three solutions containing GQD, were kept at room temperature (25°C) for 48 h, to trigger the reaction of GQDs with the surface hydroxyl groups of the CNCs. After 48 h, CNC/GQD inclusion complex films were formed. These films were ground to a fine powder using mortar and pestle for addition into polymer composites.

### 2.3. Design and manufacture of polymer composites using GQD functionalized CNC as filler material

The composite samples were manufactured using HDPE as matrix resin. Three GQD/CNC formulations synthesized in the previous step were used to manufacture HDPE masterbatches. Powdered CNC/GQD inclusion complexes were melt blended with resin. Each master batch was further used to manufacture test planks representing different volumes of GQDs added to CNC. The experiment design included three types of GQD/CNC complexes, pristine CNC incorporated and control (only HDPE) with five replications (Table 1). Composite samples were prepared by melt blending in a Thermo Fisher Scientific HAAKE Minilab II dual screw extruder (Bozeman, MT, USA). Samples were extruded at 100 rpm and 145°C for 5 minutes. After mixing, composites were injection molded into a Thermo Fisher Scientific Minijet Pro injection molder. Samples were injected into either a DMA sample mold (Thermo Fisher Scientific, Waltham, MA USA, Part # 557-2295) with dimensions of 60 mm × 10 mm × 1 mm or a tensile test dog bone mold (Thermo Fisher Scientific, Waltham, MA USA) of the geometry described in ASTM D1708.

### 2.4. Characterization

#### 2.4.1. Zeta potential measurement

The electro-kinetic potentials (ζ-potential) of GQDs, CNCs and GQD/CNC were measured using a Zeta-sizer Nano instrument (Bozeman, MT, USA), at 22.7°C and pH 7.

#### 2.4.2. Raman spectroscopy

The chemical structure and functional groups of the CNC/GQD inclusion complexes were analyzed using a Horiba LabRam HR Evolution NIR Raman microscope (Bozeman, MT, USA). A 50 × LWD objective, a stigmatic spectrometer with a grating of 300 gr/mm, and a 532 nm 450 mW laser at 0.01-1% power was used to acquire the Raman spectra. The wavenumber range was 900-3000 $cm^{-1}$, to detect the D ɬ 1350 $cm^{-1}$) and G ɬ 1583 $cm^{-1}$) peaks of graphene.

#### 2.4.3. X-ray photoelectron spectroscopy (XPS)

The chemical composition and binding energy of different chemical bonds of CNC/GQD inclusion complexes were analyzed using an X-Ray002 400 μm-FG ON with a monochromatic Al Kα source (Fargo, ND, USA). Measurements were taken at a spot size of 400 × 400 μm and the incoming photons were set to 200 eV with a step size of 1 eV.

#### 2.4.4. X-ray diffraction (XRD) analysis

XRD analysis was carried out to study the crystallographic structure of the CNC/GQD hybrid system. X-ray diffraction patterns of CNC and CNC/GQD inclusion complexes were obtained from an X-ray powder diffraction spectrometer with Cu Kα X-ray, the wavelength of 1.5418 Å (Bozeman, MT, USA). The stage was set to collect the diffraction pattern from $2\theta = 5^{\circ}$ to $70^{\circ}$.

#### 2.4.5. Field emission scanning electron microscopy (FESEM)

The composites were cryo-fractured in liquid nitrogen and the fractured surface's morphology was analyzed using SEM. Using a field

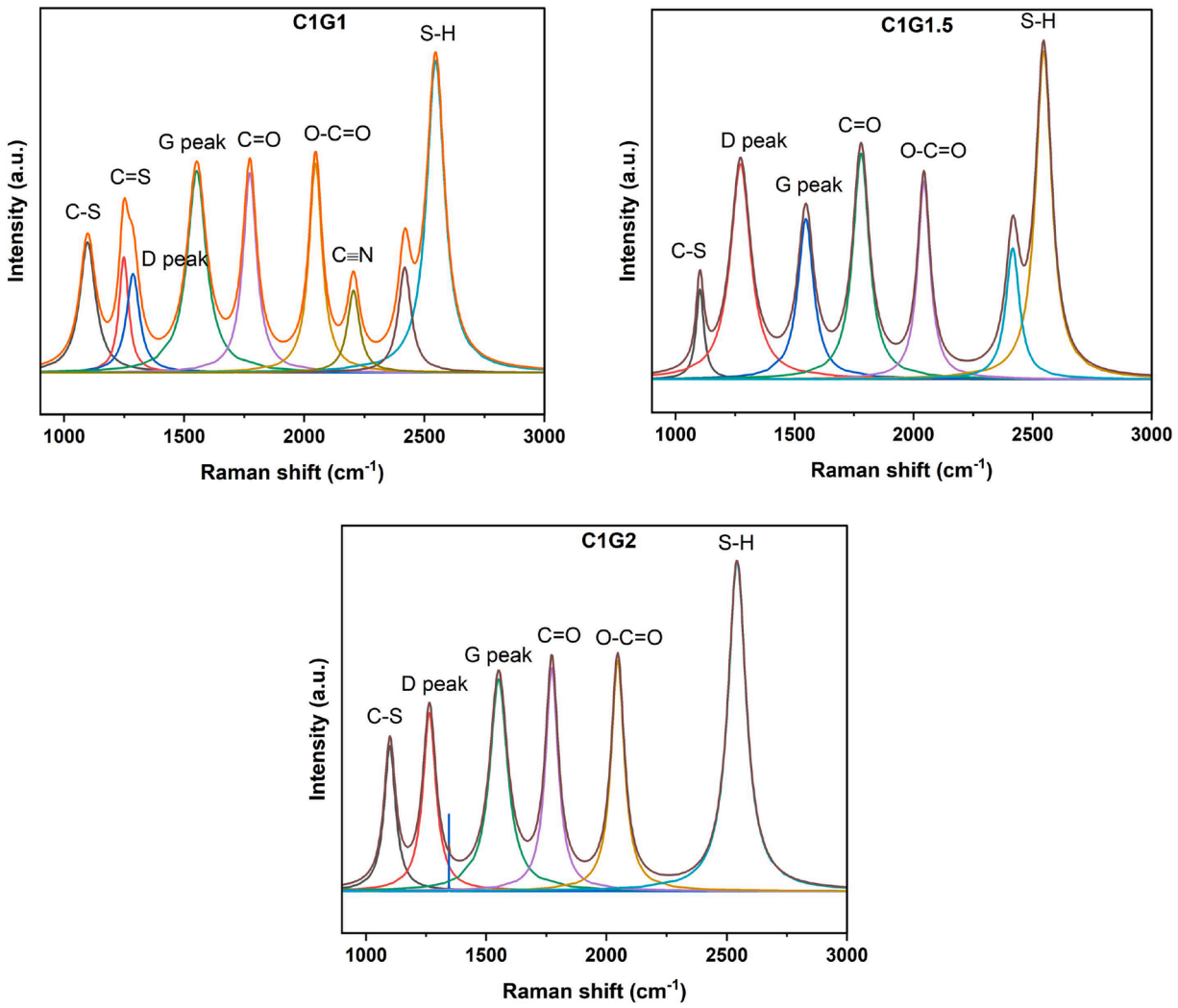


**Fig. 1.** Raman spectra of GQD/CNC inclusion complexes

emission scanning electron microscope (Supra 55VP, Zeiss, Thornwood, NY, USA), operating at an accelerating voltage of 5.0 kV, images of cross-section morphology were taken at different magnifications in the Image and Chemical Analysis Laboratory (ICAL) at Montana State University. A thin film of Iridium was created on the cross-section surface of the samples for 60 s for conductivity before capturing the images.

*2.4.6. Thermogravimetric analysis (TGA)*

TGA was used to analyze the thermal stability of composites. A TA Instruments Thermogravimetric Analyzer (TGA Q5000, New Castle, USA) at Montana State University was used to test the samples in thermal degradation mode, under a flowing nitrogen atmosphere with a 60 ml/min flow rate, from 30 °C to 600 °C, at a heating rate of 10 °C/min.

*2.4.7. Differential scanning calorimetry (DSC)*

The crystallization behavior of the composites was analyzed using DSC analysis. A TA Instruments DSC (DSC2A-01552) under a nitrogen atmosphere at Montana State University was used to measure the samples' melt peak and fusion enthalpy. Samples weighing 4-5 mg were taken and scanned over a temperature range from 30 °C to 400 °C at a heating rate of 10 °C/ min.

*2.4.8. Dynamic mechanical analysis (DMA)*

The viscoelastic behavior of the composites was studied using DMA. The samples' dynamic storage and loss modulus were measured using a TA Instruments Dynamic mechanical analyzer (Q800) (New Castle, USA) was used to measure the samples' dynamic storage and loss modulus, with the help of a three-point bending fixture. The testing conditions were as follows:hh temperature range: 30°C to 110°C, frequency of 1 Hz, amplitude of 20 μm and a force track of 125%. Two replicates were tested for each formulation and the mean values were reported.

*2.4.9. Tensile testing*

The tensile properties of the composites were measured using an MTS C43 load frame (Bozeman, MT, USA) with 5 mm/min speed and a gauge length of 35 mm from clamp to clamp. The measurements were done without using an extensometer. Five replicates were tested for each formulation and the mean values were reported.

*2.4.10. Electrical impedance spectra analysis*

The electrical behavior of the composite samples was analyzed using a four-point probe set-up and a Hioki 3533-01 LCR meter. The impedance spectra were collected using a voltage of 100 mV, within a frequency range of 4 Hz to 1 MHz. The impedance of each formulation was measured at three random points and three replicates were tested for each formulation.

**Table 2**
Characteristics of D and G bands of CNC/GQD inclusion complexes

| Sample code | $I_{DG}$ ratio | FWHM |
|---|---|---|
| C1G1 | 0.68 | 89 |
| C1G1.5 | 1.28 | 96 |
| C1G2 | 0.74 | 76 |

## 3. Results and discussion

### 3.1. Zeta potential measurement

The CNCs were negatively charged due to the presence of sulfate groups and hydroxyl groups on the surface (Li et al., 2017) and had a ζ-potential of -46.86±6.49 mV at $C_{CNC}$ = 1mg/mL, 22.7 °C and pH 7. GQDs were also negatively charged because of the carboxyl groups' deprotonation present in the edge of GQD structure (Khabibullin et al., 2017), confirmed from Raman spectroscopy and XPS, and the ζ-potential was -14.39±1.8 mV at $C_{GQD}$ = 5 mg/mL, 22.7 °C and pH 7. The increase in ζ-potential to -28.39 mV for GQD/CNCs (measured at $C_{GQD/CNC}$ = 1 mg/mL, 22.7 °C and pH 7) compared to CNC because of the hydrogen bond formation between carboxyl and hydroxyl groups of GQD and CNC respectively (Sekiya et al., 2014), also confirmed from Raman spectroscopy and XPS, indicated the formation of GQD/CNC inclusion complex.

### 3.2. Raman spectroscopy analysis of the CNC/GQD inclusion complex

Raman spectroscopy was used to investigate the chemical structure of the composites. Typically, Raman spectra of graphitic carbons show two characteristic peaks, D and G peaks. The D peak (1350 $cm^{-1}$) corresponds to the $sp^3$ carbon atom or edge defects or oxygen containing functional groups in the graphene structure. The G peak (1580 $cm^{-1}$) represents the crystallinity or the relative strength of the $sp^2$ plane (Comanescu et al., 2015). Raman spectra of all GQD incorporated composites showed both D and G peaks (Fig. 1), indicating the presence of edge defects or oxygen containing functional groups in the aromatic carbon structure (Florin et al., 2014). Generally, the D band and G band integral intensity ratio ($I_{DG}$ ratio) is used to determine the defects in the carbon structure. In this case, the $I_{DG}$ ratio increased by incorporating more GQD (Table 2). This confirmed the presence of more $sp^2$ domains in the system or more oxygen containing functional groups (Ferrari & Basko, 2013), which facilitated the reaction between surface groups of CNC and GQD.

Additionally, the change in peak position and full width of half maximum (FWHM) or line broadening of the peaks can provide insights of the graphitic structure. An apparent shift was observed in all inclusion complexes in G peak positions (1554 $cm^{-1}$). This peak shift can be associated with the increasing interaction between CNC and GQD (Budde et al., 2016). Also, the increase in the value of FWHM of the G peak indicated the peak broadening or increase in the crystal size (Florin et al., 2014), which can be confirmed from XRD analysis.

Moreover, C=S band confirmed the presence of the surface sulfate groups of CNC at 1115 $cm^{-1}$ and -S-H band at 2551 $cm^{-1}$ (Comanescu et al., 2015; Thérien-Aubin et al., 2016). After 1700 $cm^{-1}$, more oxygen containing functional groups such as carbonyl (C=O) and carboxylate group (O-C=O) was observed, which is further confirmed in XPS analysis.

The strong intermolecular interactions between the oxygen containing groups such as carboxylic acid of GQD and the surface hydroxyl groups of CNC facilitated an esterification reaction. Therefore, a strong peak at 2375 $cm^{-1}$ was observed in all GQD incorporated composites due to the presence of carboxylate group (O-C=O) (Khabibullin et al., 2017). The presence of the ester linkage in the composites also confirmed the functionalization of the CNC surface groups using GQD.

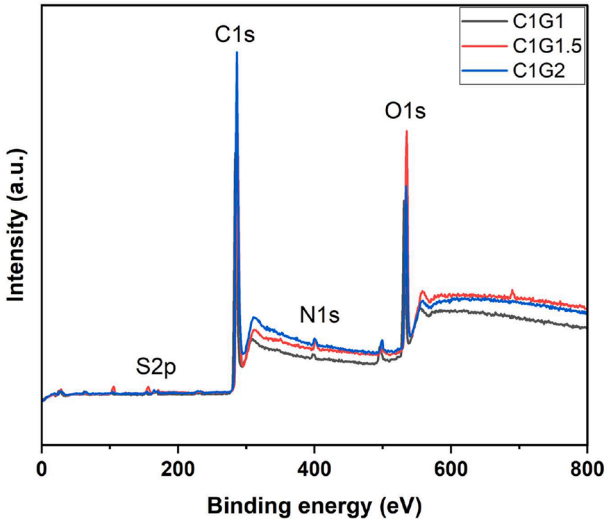


**Fig. 2.** XPS survey spectra of CNC/GQD inclusion complex.

**Table 3**
Atomic percentages of different elements in CNC/GQD inclusion complex.

| Sample code | C (atm. %) | O (atm. %) | N (atm. %) | S (atm. %) |
|---|---|---|---|---|
| C1G1 | 77.57 | 19.28 | 1.345 | 0.68 |
| C1G1.5 | 70.47 | 24.04 | 1.745 | 0.41 |
| C1G2 | 80.85 | 16.52 | 1.34 | 0.58 |

**Table 4**
O to C ratio and FWHM of CNC/GQD inclusion complex

| Sample code | O/C ratio | FWHM |
|---|---|---|
| C1G1 | 0.248 | 2.16 |
| C1G1.5 | 0.341 | 3.53 |
| C1G2 | 0.205 | 3.45 |

### 3.3. XPS analysis of CNC/GQD inclusion complex

Through XPS analysis, the surface composition of the GQD/CNC inclusion complex was explored. The XPS survey spectra of all four CNC/GQD inclusion complexes presented three peaks: a C1s peak ϵ 285 eV), an O1s peak ϵ 532 eV), an N1s peak (400 eV) and an S2p peak ϵ 168 eV), along with traces of Na and Si due to impurities in the system (Fig. 2. Table 3 and 4 display the atomic percentages of individual elements and O to C ratio. Additionally, a slight shift in peak positions indicated changes in the elemental and chemical compositions. Table 4 also showed that the FWHM value demonstrated the number of chemical bonds that contributed to the peak shape (Xiong et al., 2018).

The lower O-to-C ratio value indicated the successful chemical reactions between CNC and GQD (Xiong et al., 2017). The increase in the value of FWHM confirmed the presence of more chemical bonds in the system, indicating a more intense chemical reaction between CNC and GQD (Thomas et al., 2018).

The high resolution C1s spectra of C1G1 can be divided into three peaks. A $sp^2$ hybridized carbon (C-C) at 284.68 eV in the graphene network, $sp^3$ C (C-O-C) at 286 eV and at 288.48 eV a peak of carboxylate group (O-C=O). The same peaks are observed in the case of C1G1.5 C1s spectra (Fig. 3). In the case of C1G2, both $sp^2$ and $sp^3$ hybridized carbons were observed along with a carbonyl group (C=O) (Peng et al., 2012). All these peaks were also observed in Raman spectroscopy.

The functional groups containing oxygen atoms in GQD and the aromatic $sp^2$ domains facilitated the crosslinking reaction between GQD and CNC which is confirmed by the presence of the carboxylate group in

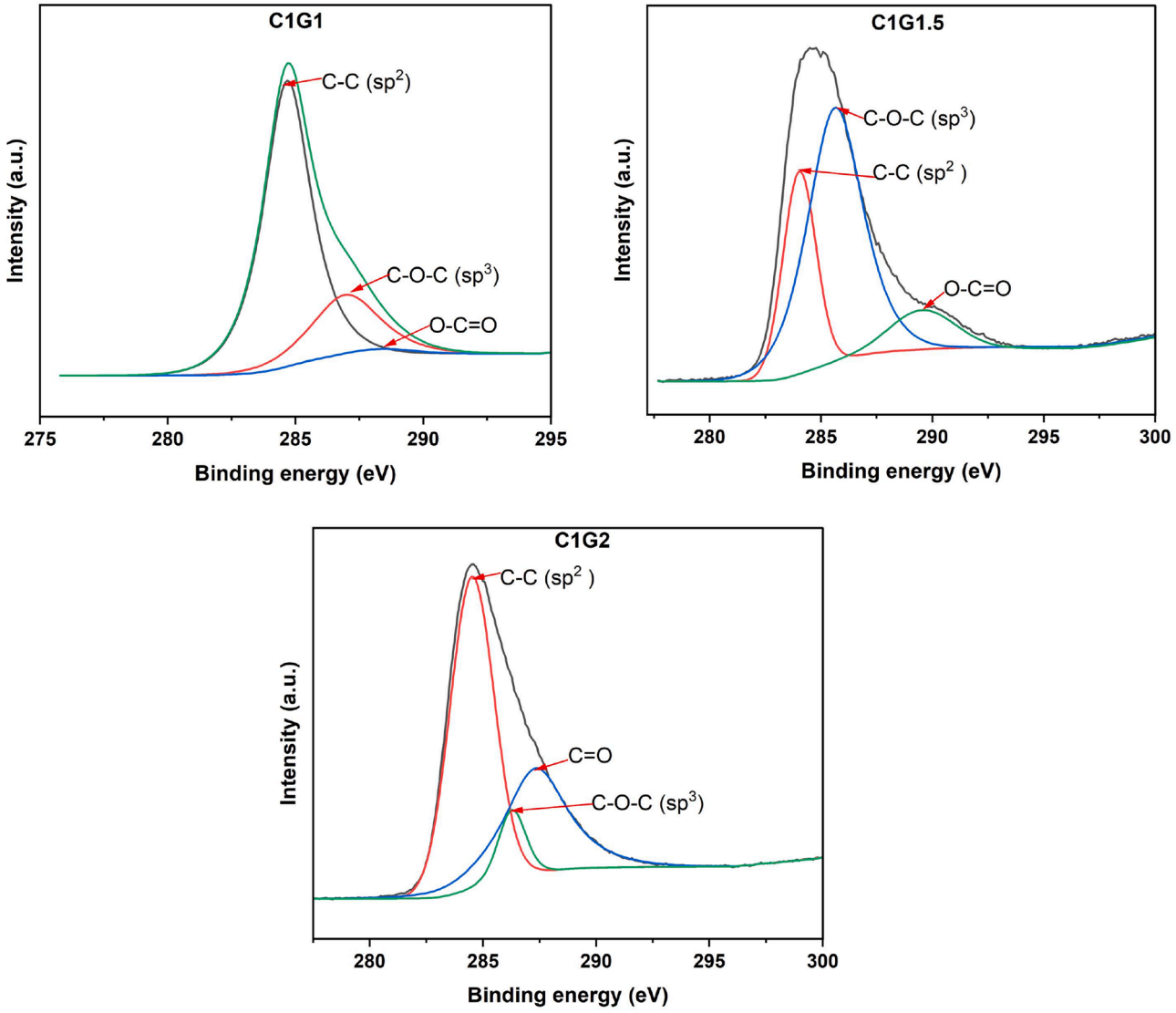


**Fig. 3.** High resolution C1s spectra of CNC/GQD inclusion complexes.

the chemical structure of the composites, which is already confirmed in the Raman Spectroscopy analysis (Khabibullin et al., 2017). Also, the peak centers changed their positions slightly, indicating the covalent reaction between CNC and GQD. The oxygen containing groups facilitated the excellent dispersion of GQDs in water and acted as potential reaction sites for CNCs (Tang et al., 2013).

### *3.4. XRD pattern analysis of CNC/GQD inclusion complex*

The crystallographic structure and crystallinity index of the CNC/GQD inclusion complex and pristine CNC were evaluated by XRD pattern analysis.

The interlayer spacing or d-spacing was calculated by using Bragg's equation and the crystallite size was calculated using the Debye-Scherrer equation (Wu et al., 2012). The XRD spectra of CNC showed three characteristic peaks of cellulose I, identified at $2\theta = 16.34°$, 22.53° and 34.47° of (110), (200) and (400) lattice planes (Tian et al., 2019). The average crystallite size was calculated using Debye-Scherrer formula and the crystallite size of CNC was 21.78 nm with a crystallinity index of 36.31%. According to the calculation of Bragg's equation, CNC's interlayer spacing (d-spacing) was 0.394 nm.

The XRD spectra of the CNC/GQD inclusion complex showed intense and sharper peaks compared to pure CNC, which indicated the

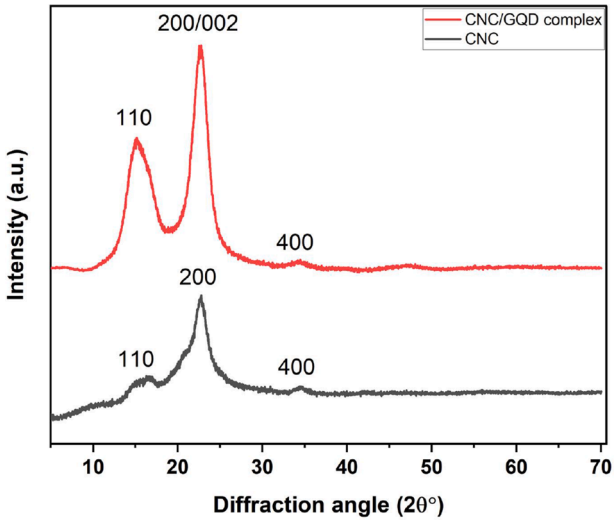


**Fig. 4.** X-Ray diffraction patterns of CNC and CNC/GQD inclusion complex.

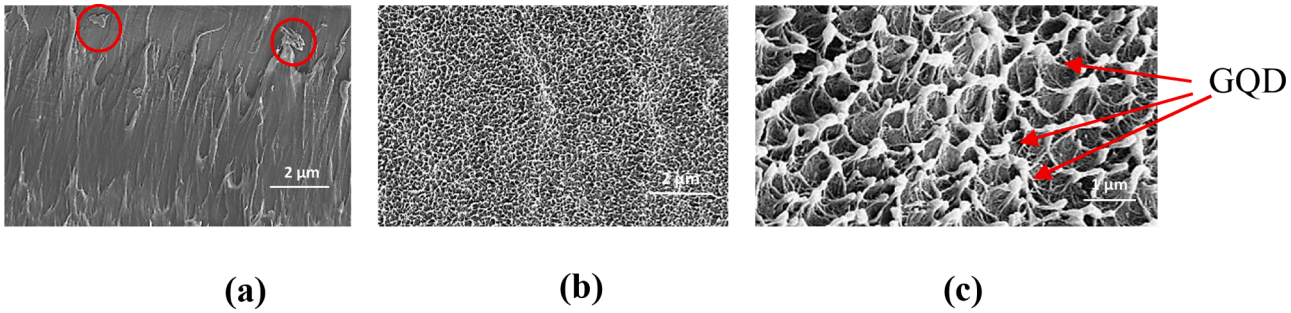


**Fig. 5.** SEM micrographs of the cryo-fractured cross-sections of (a) HDPE/CNC (2 μm), (b) HDPE/CNC/GQD (2 μm) (11,000 X) and (c) HDPE/CNC/GQD (1 μm) (56,000 X).

**Table 5**
Thermal properties of the formulations (CNC/GQD) from TGA.

| Sample code | $T_{onset}$ (°C) | $T_{50}$ (°C) | $T_{endset}$ (°C) | Residue (wt%) |
|---|---|---|---|---|
| Neat HDPE | 404.05 | 460.24 | 481.70 | 0.38 |
| C1G0 | 405.23 | 462.82 | 481.80 | 0.49 |
| C1G1 | 421.98 | 478.75 | 498.75 | 1.99 |
| C1G1.5 | 424.83 | 481.12 | 500.45 | 2.86 |
| C1G2 | 426.53 | 482.26 | 499.89 | 2.327 |

successful reaction between CNC and GQD (Waje et al., 2010). The diffraction peak of pure GQD corresponding to the (002) plane overlapped with the (200) plane of CNC (Fig. 4). The intensity of the peak increased, indicating the presence of many oxygen-containing functional groups in the system (Wu et al., 2012). The peak corresponding to the (110) plane of CNC/GQD complex also showed increased intensity compared to the pristine CNC. The change in intensity of the peaks was also known as size and edge effects of GQDs, which was previously confirmed from Raman spectroscopy and XPS analysis.

The average crystallite size of the CNC/GQD inclusion complex was 33.30 nm with an average crystallinity index of 78.68%. Larger crystallite size indicated slower nucleation and faster growth rates, resulting in a higher degree of crystallinity (Waje et al., 2010). Moreover, larger crystallite size and higher crystallinity index of the inclusion complex indicated better thermal stability of the system (Waje et al., 2010), which is further confirmed in TGA analysis of composites.

### 3.5. Morphological study of the composites

The SEM micrographs of the cryo-fractured composites' cross-sections are displayed in Fig. 5. The composites with untreated CNC exhibited agglomerations in the polymer matrix. Conversely, the composites with GQD demonstrated improved dispersion behavior, as evidenced by the absence of agglomeration in the matrix.

The cross-section of the GQD incorporated composites revealed a uniform fibrillar structure that indicated the separation and distribution of the CNCs throughout the matrix. Production of composites presents a greater challenge in the dispersion of nanomaterials since the flow of the molten polymer and the filler in the extruder is uncontrollable. The cross-section images also revealed the CNCs interacted strongly with GQDs, which led to slight entanglement of the nanofibrils as indicated by the network structure of the composites. Recent studies (Peng et al., 2012; Tang et al., 2013; Thomas et al., 2018; Tian et al., 2019; Waje et al., 2010; Wu et al., 2012) that used pristine or doped GQD as a reinforcement for composites, presented a similar morphology as the current study. In this research, the interaction between CNC and GQD overcame the issue of agglomeration and displayed synergistic behavior, due to the hydrogen bond formation and mutual electrostatic repulsion that aided in improving their dispersion in the composites (Khabibullin et al., 2017).

### 3.6. Thermogravimetric property analysis

The effect of GQD incorporation on the thermal properties of HDPE was analyzed and the results are shown in table 5. A single-step

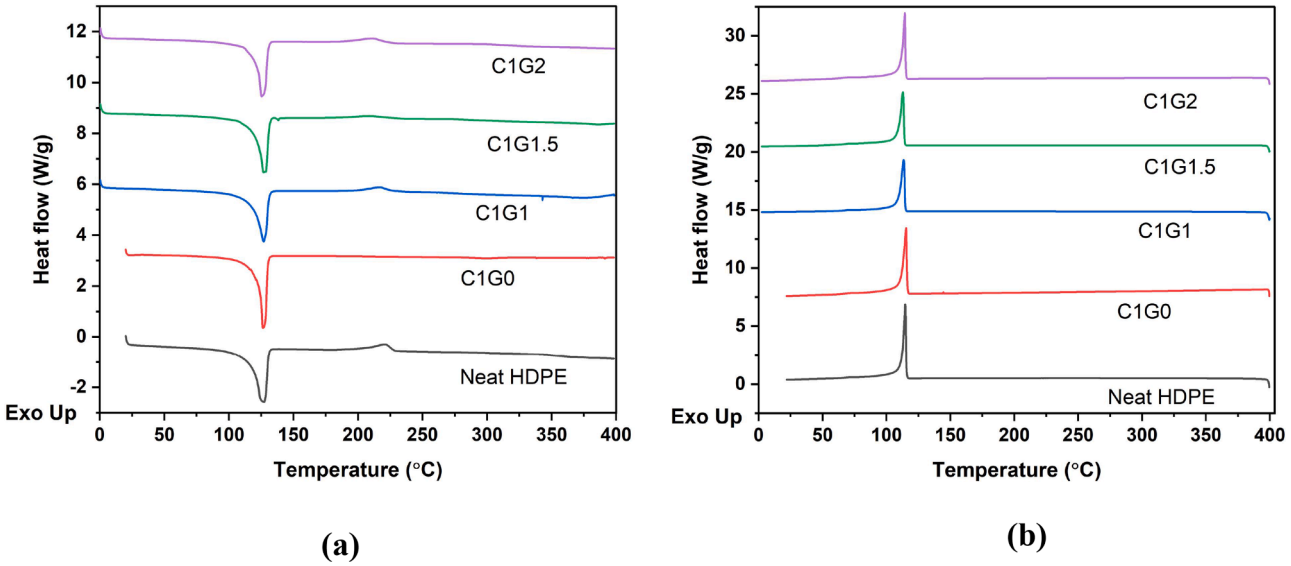


**Fig. 6.** DSC thermograms of composite samples of (a) heating cycle and (b) cooling cycle.

**Table 6**
Crystallization behavior of the formulations from DSC.

| Sample code | $T_c$ (°C) | $T_m$ (°C) | Crystallinity ($X_c$) (%) |
|---|---|---|---|
| Neat HDPE | 114.54 | 127.53 | 34.61 |
| C1G0 | 115.38 | 126.31 | 39.42 |
| C1G1 | 113.42 | 126.91 | 42.89 |
| C1G1.5 | 112.77 | 126.72 | 43.73 |
| C1G2 | 114.35 | 125.32 | 44.47 |

degradation in the TGA curves was observed for all formulations. The thermal stability of the samples was analyzed by comparing the $T_{onset}$, $T_{50}$, $T_{endset}$ values. The initial degradation temperature at which the composites start degrading represents $T_{onset}$, at 50% weight loss $T_{50}$ is measured and $T_{endset}$ represents the temperature at the end of degradation. The C1G0 composite, which only had pristine CNCs as filler material, showed no increase in $T_{onset}$ because of the catalytic nature of the sulfate groups present in CNC surface. The incorporation of GQD exhibited a higher $T_{onset}$, $T_{50}$, $T_{endset}$ values than the neat HDPE and C1G0.

The improved dispersion of the nanofillers and uniformity of the nanocomposite structure are the key factors for modest improvement in thermal properties of the composites. The incorporation of GQD enhanced the strength of the produced char layer, which in turn formed a protective barrier on the exposed polymer surface (Yu et al., 2019). Also, graphene can form multiple and overlapped char layers which promote the "labyrinth effect" or a tortuous path. This tortuous path delayed the exchange of heat/mass transfer between the condensed and gaseous phases and improved the thermal stability of the composites (Frone et al., 2013; Katti et al., 2018; Zhao et al., 2019). Thus, the cycle of mass and heat transfer was interrupted. As a result, the polymer degradation slowed down.

Moreover, the oxygen containing groups of graphene, especially the carboxylate group, facilitated self-decomposition and dehydration at lower temperatures which can lead to the adsorption of heat and cooling of the polymer substrate. This phenomenon prompted the dilution of oxygen concentration around the ignition atmosphere (Hu et al., 2014; Qian et al., 2013). Therefore, the presence of GQD in the composites improved the overall thermal stability of the system.

### 3.7. Crystallization behavior analysis of the composites

DSC was used to study the non-isothermal crystallization behavior of the HDPE composites. The DSC results are shown in Fig. 6, and Table 6. The crystallinity ($X_c$) was determined by the following equation:

$$X_c(\%) = \Delta H_m \times 100 / \Delta H_m^0 \times (1 - x) \quad (1)$$

where $\Delta H_m$ is the melting enthalpy, $\Delta H_m^0$ is the theoretical enthalpy of 100% crystalline HDPE (293 J $g^{-1}$), and x is the weight fraction of filler (CNC or CNC/GQD) (Frone et al., 2013).

The incorporation of CNC as a filler in the HDPE matrix showed an increase in crystallinity (%). The potential reason behind this change is CNC's nucleation effect, which promoted heterogeneous nucleation. The nanofillers acted as the nuclei for the heterogeneous nucleation and decreased the free energy barrier to accelerate the crystallization process (Xu et al., 2013). The nanocrystals hindered the chain diffusion due to their confinement effect and folded at the crystal growth front to promote the formation of thinner spherulites (Ying et al., 2018).

The addition of GQD also slightly improved the crystallinity of the system compared to neat HDPE. The introduction of GQDs restricted the mobility of the polymer chains, due to improved interfacial interaction between the filler and the polymer matrix. Here, GQD behaved as a dispersing agent and facilitated the dispersion CNCs in the polymer matrix (Xu et al., 2013). The crystallinity (%) of GQD incorporated composites is much lower than the crystallinity (%) of the CNC/GQD complex itself. The larger nucleus size (33.30 nm) than the pristine GQD

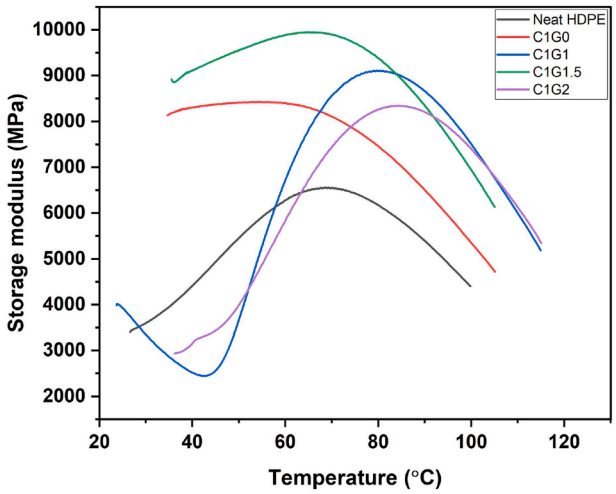


**Fig. 7.** Representative curves of storage modulus as a function of temperature of composite samples.

**Table 7**
Dynamic mechanical properties and mean comparison (Fisher LSD) of composites **(p= 0.05).**

| Sample code | Mean | Groups | Groups |
|---|---|---|---|
| C1G1 | 9487 | A | |
| C1G0 | 9451 | A | |
| C1G2 | 9442 | A | |
| C1G1.5 | 9297 | A | |
| Neat HDPE | 6462 | | B |

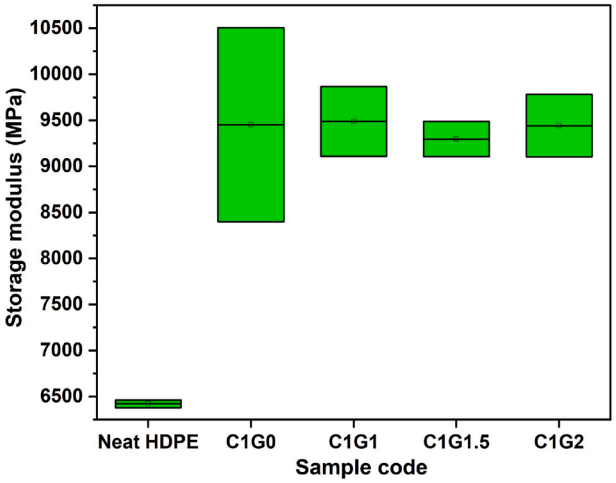


**Fig. 8.** Representative box plots of the statistical analysis of the storage modulus of the composite samples.

(10 nm), calculated from the XRD analysis, inhibited the growth rate of the crystal formation (Shojaeiarani et al., 2019) and resulted in lower crystallinity (%) of the GQD incorporated composites.

### 3.8. Dynamic mechanical behavior analysis of the composites

The dynamic viscoelastic properties were evaluated using DMA analysis. The results are shown in Fig. 7 and Table 7. For pure HDPE, a sharp α-transition peak was observed at around 68.5 °C in the storage modulus curve. In a semi-crystalline polymer like HDPE, the relaxation process is associated with long range motion of chain segments (Sewda & Maiti, 2013). GQD incorporated composites showed a higher

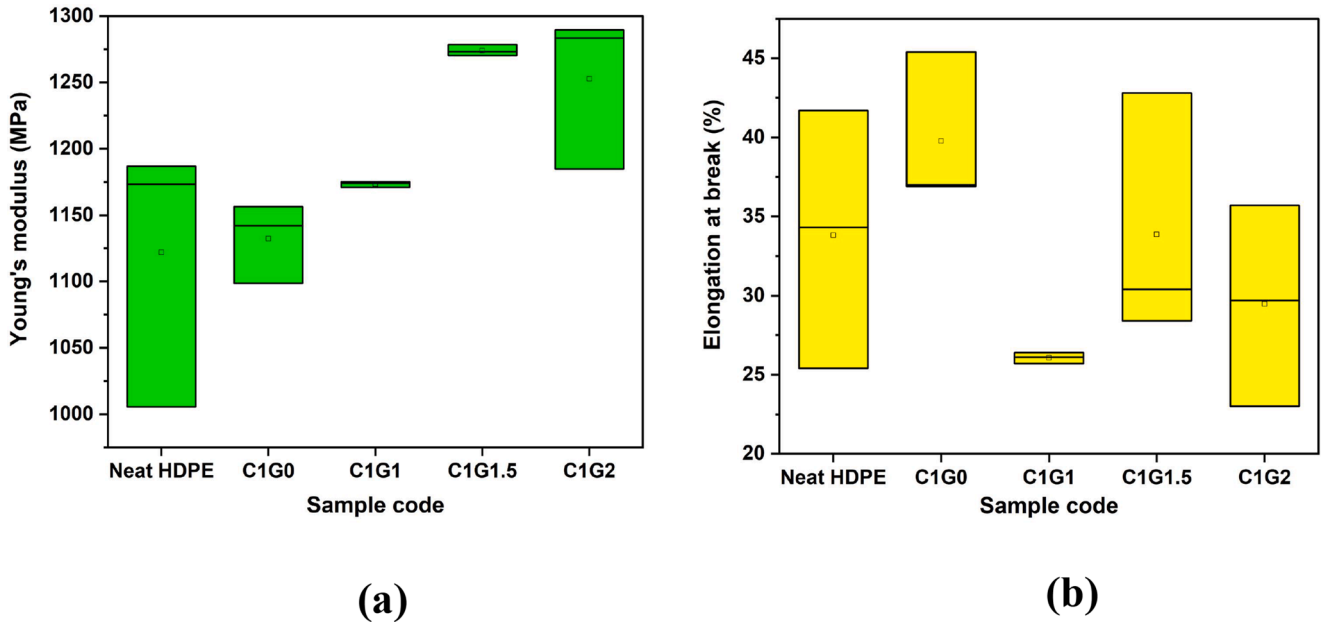


**Fig. 9.** Representative box plots of statistical analysis of (a) elastic modulus and (b) elongation at break (%) of HDPE composites.

transition temperature, around 80°C. The higher temperature indicated the increased intermolecular forces, interchain attraction and cross-linking reaction between CNC and GQD due to the presence of oxygen-containing polar groups. This increased interaction reduced the free volume of the system, thus resulting in a higher transition temperature (Min et al., 2008). The higher value of transition temperature also indicated better thermal stability (Sewda & Maiti, 2013), which was previously confirmed in TGA analysis.

The storage modulus of HDPE is 6462 MPa. The composites' dynamic mechanical properties largely depend on the filler content. Incorporation of CNC increased the storage modulus value (9451.5 MPa) significantly (Table 7 and Fig. 8). The incorporation of CNC makes the polymer chains less mobile and increases the flow resistance of HDPE (Baatti et al., 2020).

The incorporation of GQD did not show any significant impact on the dynamic mechanical properties of the composites, compared to pristine CNC incorporated composites. However, the mechanical properties are significantly higher than neat HDPE. Overall, the composites have a 46% increase in storage modulus compared to neat HDPE.

The elastic response ability of GQD incorporated composites decreased rapidly with the increase in temperature, after the transition region. At higher temperature, the gap between the graphene layers, which acted as the binding points of the polymer chains, was increased, and prompted decreased elastic response of the polymer chains (Li et al., 2017). On the other hand, the CNCs present in the inclusion complex hindered the chain slippage. Due to these two contradictory phenomena, the overall mechanical properties of the GQD incorporated composites did not improve.

### 3.9. Tensile property analysis of the composites

The mechanical property analysis such as Young's modulus, and elongation at break, were investigated to gain an insight into the tensile behavior of the composites, the effect of CNC and GQD on the tensile properties and comparison of the tensile properties with neat HDPE. Theoretically, adding CNC to a polymer matrix as a filler should improve the tensile properties of the composites (Bajwa et al., 2021). Nevertheless, like all the nanofillers, there was difficulty while mixing the CNC with the polymer (Ishak & Hafizi, 2018). But, CNCs show a self-agglomeration behavior in the polymer matrix (Xiong et al., 2017)

**Table 8**
Young's modulus and mean comparison (Fisher LSD) of each formulation (CNC/ GQD) **(p= 0.05).**

| Sample code | Mean | Groups | Groups | Groups |
|---|---|---|---|---|
| C1G1.5 | 1273.93 | A | | |
| C1G2 | 1252.49 | A | B | |
| C1G1 | 1173.31 | | B | C |
| C1G0 | 1132.33 | | | C |
| Neat HDPE | 1121.95 | | | C |

**Table 9**
Elongation at break (%) and mean comparison (Fisher LSD) of each formulation (CNC/ GQD) **(p= 0.05).**

| Sample code | Mean | Groups | Groups |
|---|---|---|---|
| C1G0 | 39.77 | A | |
| C1G1.5 | 33.87 | A | B |
| Neat HDPE | 33.8 | A | B |
| C1G2 | 29.47 | A | B |
| C1G1 | 26.07 | | B |

which can play an essential role in the tensile properties of the composites.

In the current research, CNC and GQD were incorporated in different ratios to observe and analyze their effect on the mechanical properties of HDPE polymer. The results are shown in Fig. 9, and Tables 8 and 9.

In the statistical analysis of the tensile properties of the composites, it can be observed that there is no significant difference in the elastic modulus of C1G0 composites and neat HDPE. This phenomenon can be attributed to the self-agglomeration behavior of CNC in the hydrophobic matrix, which reduced the filler/matrix interaction (Xiong et al., 2021). The significant difference in the elongation of C1G0 and C1G1 composites also supported the hypothesis of the agglomeration of CNC in the polymer matrix.

On the other hand, the GQD incorporated samples showed a significant improvement in the elastic modulus of the composites. The filler/matrix interface, nanofillers' dispersion, and nanocomposite structure's uniformity played a significant role in the improvement of the tensile properties of the composites. The uniform dispersion of fillers leads to an effective stress transfer, producing a stronger composite (Bajwa et al.,

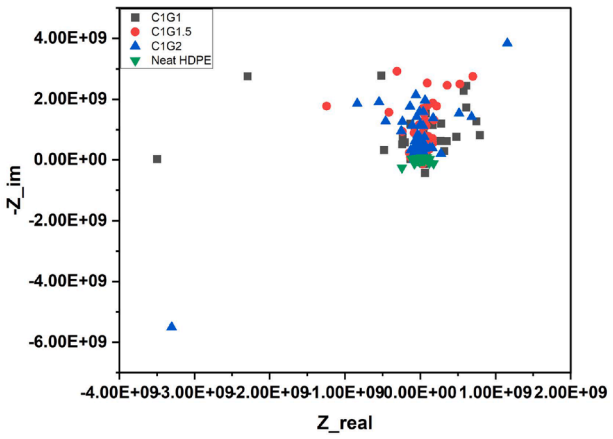


**Fig. 10.** Nyquist plot for electrical impedance spectra of neat HDPE and CNC/GQD composites.

2021).

In the SEM micrographs, no agglomeration was observed, and the composites had a uniform honeycomb like structure. The lack of agglomeration and uniform distribution of fillers throughout the matrix helped to improve the elastic modulus of the composites. Incorporation of GQD did not decrease the elongation of the composites compared to neat HDPE, which is useful for high impact resistant composites, thanks to the layered structure of graphene (Khabibullin et al., 2017). Overall, there is a 13% increase in elastic modulus in the case of GQD incorporated composites compared to neat HDPE.

### 3.10. *Electrical impedance spectra analysis*

One of the recent application areas of graphene-based materials is energy storage devices. The high surface area, thermal and chemical stability, conductivity, and charge carrier mobility of graphene facilitate the accumulation and charge storage, which is the fundamental requirement of energy storage devices. Graphene based materials can be used in the coatings of capacitor plates to produce an electric double-layer coating (Xiong et al., 2021). GQD, a graphene-based material, is a potential candidate for energy storage devices in combination with CNC. The large number of functional groups on the surface of GQD, such as -COOH, -OH, -$NH_2$, can perform as active coordination sites for transition metal ions (Talapin et al., 2010). GQD based energy storage devices have an electro-chemical double-layer and adsorb charges on the surface of the electrodes (Shinde & Pillai, 2013; Zhang et al., 2013). On the other hand, CNC is biocompatible, eco-friendly, and thermally stable (Huang et al., 2013). These intriguing properties of CNC/GQD composites should be explored in the future to unlock their potential to be used as energy storage devices.

All the GQD induced composites and neat HDPE showed a purely capacitive AC electrical behavior. In an AC system for a capacitor, reducing the frequency leads to a higher impedance value (Z). Therefore, a capacitor has very little or no contribution towards Z at a very high frequency, and at a low frequency, the Z value becomes infinite. As a result, the Bode plot of an ideal capacitor shows a constant phase shift of 90° and a linear curve with a negative slope for Z (Jung et al., 2015). In the current study, all the GQD induced composites and HDPE showed an average phase shift of 90° and a negative slope linear curve for Z (Fig. 11).

The limited imaginary component of impedance (-$Z_{im}$) was observed for all composites and HDPE in the Nyquist plot (Fig. 10). For a purely capacitive behavior, the Nyquist plot showed a straight line for the imaginary component parallel to the ordinate (Fang et al., 2014), similar to the current study.

However, the GQD content being too small, no conductive response was observed for the composites. If the GQD content is increased, a continuous network structure will be generated to facilitate the formation of a conductive path (Talapin et al., 2010; Zhang et al., 2013). The potential of CNC/GQD composites as a capacitor can be explored further in future.

## 4. Conclusion

To enhance the physical and thermo-mechanical properties of widely used HDPE polymer various types of bio-based nanofillers are incorporated into the matrix. The dispersion of nano-fillers in the polymer matrix plays the most pivotal role in their mechanical properties. The current study investigated the role of GQD as a dispersing agent and its effect on the thermo-mechanical properties of composites. In this research, CNC was successfully functionalized with GQD and CNC/GQD inclusion complex was used as filler/reinforcement to produce composites via the melt blending extrusion process. The reaction between CNC and GQD was carefully studied and confirmed by Raman spectroscopy, XPS and XRD analysis. The SEM micrographs of the cryo-

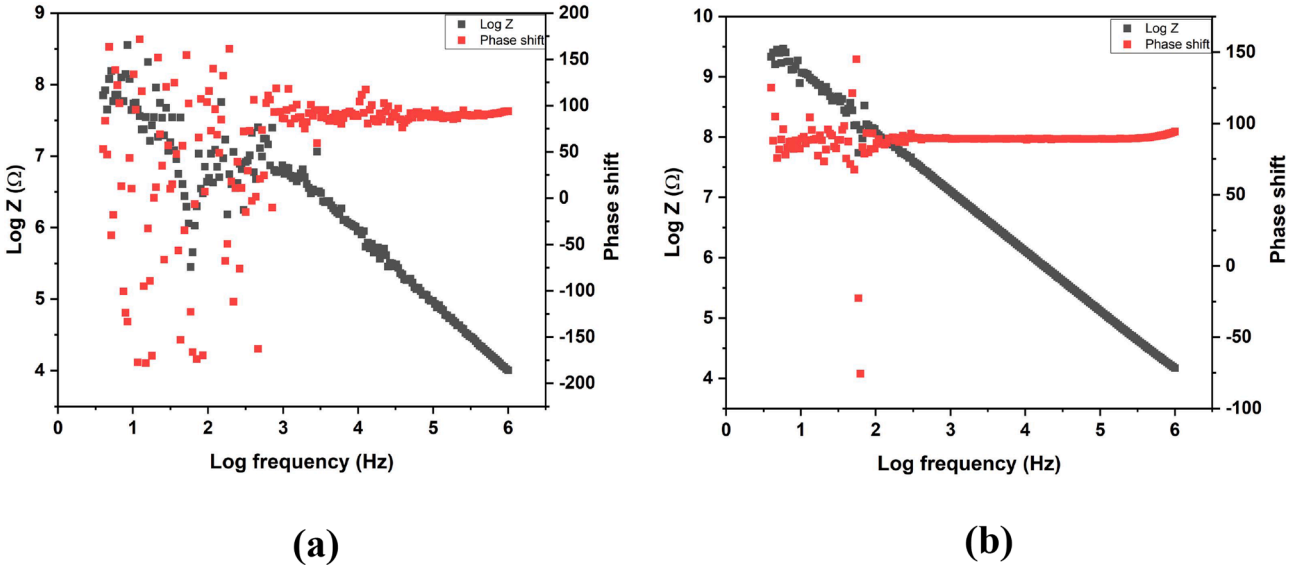


**Fig. 11.** Bode plot for electrical impedance spectra of (a) neat HDPE and (b) CNC/GQD composites.

**Table 1**
Formulations of the composite samples.

| Sample code | Resin (HDPE)(wt%) | CNC(wt%) | GQD (g)(wt%) |
|---|---|---|---|
| Neat HDPE | 100 | - | - |
| C1G0 | 99 | 1 | - |
| C1G1 | 99 | 1 | 0.010 |
| C1G1.5 | 99 | 1 | 0.015 |
| C1G2 | 99 | 1 | 0.020 |

fractured cross-sections of the composites exhibited a uniform dispersion of fillers and a lack of agglomeration in the system. The uniform dispersion of nanofillers and structural uniformity of the composites also helped in improving thermal stability. The mechanical properties of the composites were improved due to the reinforcement effect of the CNC/GQD inclusion complex. A 46% increase in storage modulus, and a 13% increase in elastic modulus were observed in the case of the GQD incorporated composites compared to neat HDPE. The electrical impedance spectra showed a purely capacitive response of GQD induced composites. The dispersion of the nanofillers in the matrix and the thermos-mechanical properties of the composites can be further improved by optimizing the amount of GQD in the system. Application of the CNC/GQD inclusion complex as an energy storage device has great potential and can be explored in the future, (Table 1).

## CRediT authorship contribution statement

**Dilpreet S. Bajwa:** Writing – original draft, Validation, Resources, Funding acquisition. **Saptaparni Chanda:** Writing – original draft, Methodology, Investigation, Formal analysis, Data curation, Conceptualization. **Cecily Ryan:** Writing – review & editing, Validation, Formal analysis. **Sreekala G. Bajwa:** Writing – review & editing, Visualization, Supervision, Resources, Project administration, Conceptualization. **Nicole Stark:** Visualization, Resources, Methodology. **Kirsten Matteson:** Writing – original draft, Resources, Formal analysis.

## Declaration of competing interest

The authors declare that they have no known competing financial interests or personal relationships that could have appeared to influence the work reported in this paper.

## Data availability

Data will be made available on request.

## Acknowledgements

The research is funded by U.S. National Institute of Standards and Technology (NIST), grant number 70NANB18H256N.

Disclaimer: Mention of trade names or commercial products in this publication is solely for the purpose of providing specific information and does not imply recommendation or endorsement by the U.S. Department of Agriculture. USDA is an equal opportunity provider and employer.

## References

Angles, M. Neus, & Dufresne, Alain (2001). Plasticized starch/tunicin whiskers nanocomposite materials. 2. Mechanical behavior. *Macromolecules, 34*(9), 2921–2931. https://doi.org/10.1021/ma001555h

Baatti, A., et al. (2020). DMA analysis, thermal study and morphology of polymethylsilsesquioxane nanoparticles-reinforced HDPE nanocomposite. *Journal of Thermal Analysis and Calorimetry, 139*(2), 789–797.

Bajwa, Dilpreet S., et al. (2021). Role of hybrid nano-zinc oxide and cellulose nanocrystals on the mechanical, thermal, and flammability properties of poly (lactic acid) polymer. *Journal of Composites Science, 5*(2), 43.

Budde, Harald, et al. (2016). Raman radiation patterns of graphene. *ACS Nano, 10*(2), 1756–1763. https://doi.org/10.1021/acsnano.5b06631

Comanescu, Constantin Florin, et al. (2015). Micro-Raman spectroscopy of graphene transferred by wet chemical methods. In *2015 International Semiconductor Conference (CAS)*. IEEE.

Eichhorn, S. J., & Davies, G. R. (2006). Modelling the crystalline deformation of native and regenerated cellulose. *Cellulose, 13*(3), 291–307. https://doi.org/10.1007/s10570-006-9046-3

Fang, Zhiqiang, et al. (2014). Novel nanostructured paper with ultrahigh transparency and ultrahigh haze for solar cells. *Nano Letters, 14*(2), 765–773. https://doi.org/10.1021/nl404101p

Ferrari, Andrea C., & Basko, Denis M. (2013). Raman spectroscopy as a versatile tool for studying the properties of graphene. *Nature Nanotechnology, 8*(4), 235–246. https://doi.org/10.1038/nnano.2013.46

Florin, Comanescu Constantin, Dinescu, Adrian, & Purica, Munizer (2014). Raman spectroscopy investigation of electron beam irradiated graphene. In *2014 International Semiconductor Conference (CAS)*. IEEE.

Frone, Adriana N., et al. (2013). Morphology and thermal properties of PLA–cellulose nanofibers composites. *Carbohydrate Polymers, 91*(1), 377–384. https://doi.org/10.1016/j.carbpol.2012.08.054

Gobi, Navathej, et al. (2017). Infusion of graphene quantum dots to create stronger, tougher, and brighter polymer composites. *ACS Omega, 2*(8), 4356–4362.

Guo, Jiaqi, et al. (2017). Photoluminescent hybrids of cellulose nanocrystals and carbon quantum dots as cytocompatible probes for in vitro bioimaging. *Biomacromolecules, 18*(7), 2045–2055. https://doi.org/10.1021/acs.biomac.7b00306

Habibi, Youssef, Lucia, Lucian A., & Rojas, Orlando J. (2010). Cellulose nanocrystals: Chemistry, self-assembly, and applications. *Chemical Reviews, 110*(6), 3479–3500. https://doi.org/10.1021/cr900339w

Habibi, Youssef. (2014). Key advances in the chemical modification of nanocelluloses. *Chemical Society Reviews, 43*(5), 1519–1542. https://doi.org/10.1039/C3CS60204D

Hu, W., et al. (2014). Covalent functionalization of graphene oxide with flame retardant and its effect on thermal stability and flame retardancy of epoxy composites. *International Association, 11*, 895–904.

Huang, Jia, et al. (2013). Highly transparent and flexible nanopaper transistors. *ACS Nano, 7*(3), 2106–2113. https://doi.org/10.1021/nn304407r

Ikram, Muhammad, et al. (2022). Photocatalytic and antibacterial activity of graphene oxide/cellulose-doped TiO 2 quantum dots: In silico molecular docking studies. *Nanoscale Advances, 4*(18), 3764–3776.

Ishak, Wan, Hafizi, Wan, et al. (2018). Gamma irradiation-assisted synthesis of cellulose nanocrystal-reinforced gelatin hydrogels. *Nanomaterials, 8*(10), 749. https://doi.org/10.3390/nano8100749

Iwamoto, S., Nakagaito, A. N., & Yano, H. (2007). Nano-fibrillation of pulp fibers for the processing of transparent nanocomposites. *Applied Physics A, 89*(2), 461–466. https://doi.org/10.1007/s00339-007-4175-6

Jung, Yei Hwan, et al. (2015). High-performance green flexible electronics based on biodegradable cellulose nanofibril paper. *Nature Communications, 6*(1), 7170. https://doi.org/10.1038/ncomms8170

Junka, Karoliina, et al. (2014). Modification of cellulose nanofibrils with luminescent carbon dots. *Biomacromolecules, 15*(3), 876–881. https://doi.org/10.1021/bm4017176

Kargarzadeh, Hanieh, et al. (2017). Recent developments on nanocellulose reinforced polymer nanocomposites: A review. *Polymer, 132*, 368–393. https://doi.org/10.1016/j.polymer.2017.09.043

Katti, Prajakta, et al. (2018). Poly (ether ether ketone)-grafted graphene oxide "interconnects" enhance mechanical, dynamic mechanical, and flame-retardant properties in epoxy laminates. *ACS Omega, 3*(12), 17487–17495.

Khabibullin, Amir, et al. (2017). Injectable shear-thinning fluorescent hydrogel formed by cellulose nanocrystals and graphene quantum dots. *Langmuir, 33*(43), 12344–12350. https://doi.org/10.1021/acs.langmuir.7b02906

Kumar, Sunil, Supriya, Sweety, & Kar, Manoranjan (2017). Multiple electrical phase transitions in Al substituted barium hexaferrite. *Journal of Applied Physics, 122*(22), Article 224106. https://doi.org/10.1063/1.4998719

Li, Yunfeng, et al. (2017). Supramolecular nanofibrillar thermoreversible hydrogel for growth and release of cancer spheroids. *Angewandte Chemie International Edition, 56*(22), 6083–6087. https://doi.org/10.1002/anie.201610353

Liu, Quanyi, et al. (2021). Recent advances in the flame retardancy role of graphene and its derivatives in epoxy resin materials. *Composites Part A: Applied Science and Manufacturing, 149*, Article 106539. https://doi.org/10.1016/j.compositesa.2021.106539

Lv, Jinling, et al. (2018). Graphene oxide-cellulose nanocrystal (GO-CNC) composite functionalized PVDF membrane with improved antifouling performance in MBR: Behavior and mechanism. *Chemical Engineering Journal, 352*, 765–773. https://doi.org/10.1016/j.cej.2018.07.088

Min, A. Min, Chuah, T. G., & Chantara, T. R. (2008). Thermal and dynamic mechanical analysis of polyethylene modified with crude palm oil. *Materials & Design, 29*(5), 992–999. https://doi.org/10.1016/j.matdes.2007.03.023

Moon, Robert J., et al. (2011). Cellulose nanomaterials review: Structure, properties and nanocomposites. *Chemical Society Reviews, 40*(7), 3941–3994. https://doi.org/10.1039/C0CS00108B

Oksman, Kristiina, et al. (2016). Review of the recent developments in cellulose nanocomposite processing. *Composites Part A: Applied Science and Manufacturing, 83*, 2–18.

Peng, Juan, et al. (2012). Graphene quantum dots derived from carbon fibers. *Nano Letters, 12*(2), 844–849. https://doi.org/10.1021/nl2038979

Qian, Xiaodong, et al. (2013). Novel organic–inorganic flame retardants containing exfoliated graphene: Preparation and their performance on the flame retardancy of

epoxy resins. *Journal of Materials Chemistry A, 1*(23), 6822–6830. https://doi.org/10.1039/C3TA10416H

Rodell, Christopher B., et al. (2015). Shear-thinning supramolecular hydrogels with secondary autonomous covalent crosslinking to modulate viscoelastic properties in vivo. *Advanced Functional Materials, 25*(4), 636–644. https://doi.org/10.1002/adfm.201403550

Rosddi, Najwa Norimanina Muhammad, et al. (2020). Cationically modified nanocrystalline cellulose/carboxyl-functionalized graphene quantum dots nanocomposite thin film: Characterization and potential sensing application. *Crystals, 10*(10), 875. https://doi.org/10.3390/cryst10100875

Sekiya, Ryo, et al. (2014). White-light-emitting edge-functionalized graphene quantum dots. *Angewandte Chemie International Edition, 53*(22), 5619–5623. https://doi.org/10.1002/anie.201311248

Sewda, Kamini, & Maiti, S. N. (2013). Dynamic mechanical properties of high-density polyethylene and teak wood flour composites. *Polymer Bulletin, 70*(10), 2657–2674. https://doi.org/10.1007/s00289-013-0941-0

Shinde, Dhanraj B., & Pillai, Vijayamohanan K. (2013). Electrochemical resolution of multiple redox events for graphene quantum dots. *Angewandte Chemie International Edition, 52*(9), 2482–2485.

Shojaeiarani, Jamileh, et al. (2019). Rheological properties of cellulose nanocrystals engineered polylactic acid nanocomposites. *Composites Part B: Engineering, 161*, 483–489.

Shojaeiarani, Jamileh, Bajwa, Dilpreet S., & Chanda, Saptaparni (2021). Cellulose nanocrystal based composites: A review. *Composites Part C: Open Access, 5*, Article 100164. https://doi.org/10.1016/j.compositesa.2015.10.041

Song, Liqing, et al. (2015). Structure observation of graphene quantum dots by single-layered formation in layered confinement space. *Chemical Science, 6*(8), 4846–4850.

Sun, Hanjun, et al. (2013). Recent advances in graphene quantum dots for sensing. *Materials Today, 16*(11), 433–442. https://doi.org/10.1016/j.mattod.2013.10.020

Talapin, Dmitri V., et al. (2010). Prospects of colloidal nanocrystals for electronic and optoelectronic applications. *Chemical Reviews, 110*(1), 389–458. https://doi.org/10.1021/cr900137k

Tang, Libin, et al. (2013). Size-dependent structural and optical characteristics of glucose-derived graphene quantum dots. *Particle & Particle Systems Characterization, 30*(6), 523–531.

Thérien-Aubin, Héloïse, et al. (2016). Temperature-responsive nanofibrillar hydrogels for cell encapsulation. *Biomacromolecules, 17*(10), 3244–3251. https://doi.org/10.1021/acs.biomac.6b00979

Thomas, Bejoy, et al. (2018). Nanocellulose, a versatile green platform: From biosources to materials and their applications. *Chemical Reviews, 118*(24), 11575–11625. https://doi.org/10.1021/acs.chemrev.7b00627

Tian, Weiqian, et al. (2019). Multifunctional nanocomposites with high strength and capacitance using 2D MXene and 1D nanocellulose. *Advanced Materials, 31*(41), Article 1902977. https://doi.org/10.1002/adma.201902977

Waje, Samaila Bawa, et al. (2010). X-ray diffraction studies on crystallite size evolution of CoFe2O4 nanoparticles prepared using mechanical alloying and sintering. *Applied Surface Science, 256*(10), 3122–3127. https://doi.org/10.1016/j.apsusc.2009.11.084

Wu, Chun-Nan, et al. (2012). Ultrastrong and high gas-barrier nanocellulose/clay-layered composites. *Biomacromolecules, 13*(6), 1927–1932. https://doi.org/10.1021/bm300465d

Xiong, Chuanyin, et al. (2021). Construction of flexible cellulose nanofiber fiber@ graphene quantum dots hybrid film applied in supercapacitor and sensor. *Cellulose, 28*, 10359–10372. https://doi.org/10.1007/s10570-021-04178-x

Xiong, Rui, et al. (2017). Template-guided assembly of silk fibroin on cellulose nanofibers for robust nanostructures with ultrafast water transport. *ACS Nano, 11*(12), 12008–12019. https://doi.org/10.1021/acsnano.7b04235

Xiong, Rui, et al. (2018). Wrapping nanocellulose nets around graphene oxide sheets. *Angewandte Chemie International Edition, 57*(28), 8508–8513.

Xiong, Rui, et al. (2019). Self-assembly of emissive nanocellulose/quantum dot nanostructures for chiral fluorescent materials. *ACS Nano, 13*(8), 9074–9081. https://doi.org/10.1021/acsnano.9b03305

Xu, Xuezhu, et al. (2013). Cellulose nanocrystals vs. cellulose nanofibrils: A comparative study on their microstructures and effects as polymer reinforcing agents. *ACS Applied Materials & Interfaces, 5*(8), 2999–3009.

Ying, Zeren, et al. (2018). Rheological and mechanical properties of polylactide nanocomposites reinforced with the cellulose nanofibers with various surface treatments. *Cellulose, 25*(7), 3955–3971. https://doi.org/10.1007/s10570-018-1862-8

Yu, Jiao, et al. (2019). Insights on the capillary transport mechanism in the sustainable cement hydrate impregnated with graphene oxide and epoxy composite. *Composites Part B: Engineering, 173*, Article 106907. https://doi.org/10.1016/j.compositesb.2019.106907

Zhang, Yan, et al. (2013). Graphene quantum dots/gold electrode and its application in living cell H 2 O 2 detection. *Nanoscale, 5*(5), 1816–1819. https://doi.org/10.1039/C3NR33954H

Zhao, Bin, et al. (2019). Functionalized Graphene Oxide Based on Hydrogen-Bonding Interaction in Water: Preparation and Flame-Retardation on Epoxy Resin. *Macromolecular Materials and Engineering, 304*(8), Article 1900164. https://doi.org/10.1002/mame.201900164